PERGAMON

International Journal of Heat and Mass Transfer 45 (2002) 1791–1806

International Journal of HEAT and MASS TRANSFER

www.elsevier.com/locate/ijhmt

Subcooled flow boiling heat transfer of R-134a and the associated bubble characteristics in a vertical plate heat exchanger

Y.Y. Hsieh, L.J. Chiang, T.F. Lin *

Department of Mechanical Engineering, National Chiao Tung University, Hsinchu 30010, Taiwan, ROC

Received 26 January 2001; received in revised form 11 September 2001

Abstract

Subcooled flow boiling heat transfer characteristics of refrigerant R-134a in a vertical plate heat exchanger (PHE) are investigated experimentally in this study. Besides, the associated bubble characteristics are also inspected by visualizing the boiling flow in the vertical PHE. In the experiment two vertical counterflow channels are formed in the exchanger by three plates of commercial geometry with a corrugated sinusoidal shape of a chevron angle of 60°. Upflow boiling of subcooled refrigerant R-134a in one channel receives heat from the downflow of hot water in the other channel. The effects of the boiling heat flux, refrigerant mass flux, system pressure and inlet subcooling of R-134a on the subcooled boiling heat transfer are explored in detail. The results are presented in terms of the boiling curves and heat transfer coefficients. The measured data showed that the slopes of the boiling curves change significantly during the onset of nucleate boiling (ONB) especially at low mass flux and high saturation temperature. Besides, the boiling hysteresis is significant at a low refrigerant mass flux. The subcooled boiling heat transfer coefficient is affected noticeably by the mass flux of the refrigerant. However, increases in the inlet subcooling and saturation temperature only show slight improvement on the boiling heat transfer coefficient.

The photos from the flow visualization reveal that at higher imposed heat flux the plate surface is covered with more bubbles and the bubble generation frequency is substantially higher, and the bubbles tend to coalesce to form big bubbles. But these big bubbles are prone to breaking up into small bubbles as they move over the corrugated plate, producing strong agitating flow motion and hence enhancing the boiling heat transfer. We also note that the bubbles nucleated from the plate are suppressed to a larger degree for higher inlet subcooling and mass flux. Finally, empirical correlations are proposed to correlate the present data for the heat transfer coefficient and the bubble departure diameter in terms of boiling, Froude, Reynolds and Jakob numbers.

1. Introduction

Subcooled flow boiling has long been recognized as one of the most effective heat transfer modes due to the simultaneous presence of a large temperature difference and boiling in the flow. Thus it has received considerable attention in the applications where highly efficient cooling is required, such as in emergency core cooling of nuclear reactors, first-wall cooling of fusion reactors, cooling of neutron generators for cancer therapy and material testing, high-power electronic cooling, and cooling of rocket nozzles.

In the following the relevant literature on the basic subcooled flow boiling heat transfer characteristics is briefly reviewed first. Subcooled flow boiling of heptane on both internally heated rod and resistance-heated coiled wire in an annular duct was examined by Müller-Steinhagen et al. [1]. Their results indicated that the boiling heat transfer coefficient increased with increasing heat flux but decreased with increasing system pressure and liquid subcooling, while independent of the mass velocity in the nucleate boiling regime. Hasan et al. [2] measured the subcooled nucleate boiling of R-113 flow

* Corresponding author. Tel.: +886-35712121x55118; fax: +886-35726440.

E-mail address: t7217@cc.nctu.edu.tw (T.F. Lin).

0017-9310/02/$ - see front matter
PII: S0017-9310(01)00294-0

Nomenclature

A	heat transfer area of the plate, m^2
Bo	Boiling number, $Bo = q/Gi_{fg}$, dimensionless
C_p	specific heat, J/kg °C
d_p	bubble departure diameter, m
D_h	hydraulic diameter, m
Fr	Froude number, $Fr = G^2/\rho_l^2 g D_h$, dimensionless
g	acceleration due to gravity, m/s^2
G	mass flux, kg/m^2 s
h	heat transfer coefficient, W/m^2 °C
i_{fg}	enthalpy of vaporization, J/kg
Ja	Jakob number based on liquid subcooling, $Ja = \rho_l C_p \Delta T_{sat}/\rho_g i_{fg}$, dimensionless
k	thermal conductivity, W/m °C
LMTD	log mean temperature difference, °C
Pr	Prandtl number, $Pr = \mu C_p/k$, dimensionless
Q	heat transfer rate, W
q	average imposed heat flux, W/m^2
R_{wall}	thermal resistance of the wall
Re	Reynolds number, $Re = GD_h/\mu_l$, dimensionless
T	temperature, °C
$T_{w,ave}$	average water temperature in the water side corresponding to the subcooled boiling region in the refrigerant side, $T_{w,ave} = (T_{w,i} + T_{w,b})/2$, °C
U	overall heat transfer coefficient, W/m^2 °C
W	mass flow rate, kg/s

Greek symbols

ΔT	temperature difference, °C
ΔT_{sat}	cross-channel superheat, $\Delta T_{sat} = T_{w,ave} - T_{sat}$, °C
ΔT_{sub}	inlet subcooling, $\Delta T_{sub} = T_{sat} - T_{r,i}$, °C
μ	viscosity, N s/m^2
ρ	density, kg/m^3
$\Delta\rho$	$= \rho_l - \rho_g$, kg/m^3
σ	surface tension, N/m

Subscripts

ave	average
b	where R-134a starts to boil
i, o	at inlet and exit of test section
l, g	liquid and vapor phase
l	all-liquid nonboiling heat transfer
r	refrigerant
single	single-phase heat transfer region in PHE
w	water
wall	wall of the plate heat exchanger
sat	saturated state
sub	subcooled state

through a vertical annular channel and showed that the boiling heat transfer coefficient was lower for higher pressure and subcooling. Moreover, the heat transfer coefficient increased with the mass velocity of the refrigerant flow. Sivagnanam et al. [3] studied subcooled flow boiling of binary mixtures on a long platinum wire and proposed correlations for the partial boiling and fully developed boiling. Subcooled flow boiling of water at high heat flux was experimentally investigated by Del Valle M. and Kenning [4]. They found that the heat transfer coefficient increased with the subcooling and heated wall thickness. Klausner et al. [5] measured the bubble departure diameter in forced convection boiling of R-113 through a rectangular channel. They noted that the mean bubble departure diameter decreased with increasing mass flux and decreasing heat flux. Chien and Webb [6] studied the bubble dynamics for pool boiling on an enhanced tubular surface and showed that the mean bubble diameter was smaller for a higher heat flux and the bubble growth period was shorter for smaller bubbles and higher heat flux. A visual study of vapor bubble growth and departure in vertical upflow and downflow forced convection boiling performed by Thorncroft et al. [7] indicated that both the bubble growth and bubble departure rates increased with the Jakob number, but decreased with the mass flux. The sliding of the bubbles on the boiling surface was found to enhance the forced convection boiling heat transfer of FC-87 by Thorncroft and Klausner [8].

The literature reviewed above is mainly focused on water and R-113. Recently, a few studies have been reported on new refrigerants such as R-134a and R-410A since they have zero ozone depletion potential and are currently recognized as the main replacement to R-12 and R-22, respectively. The subcooled flow boiling and the associated bubble characteristics of R-134a in an annular channel were measured recently by Yin et al. [9]. They showed that the subcooled boiling heat transfer was not significantly affected by the refrigerant mass flux, imposed heat flux and saturation temperature. But an increase in the subcooling resulted in much better heat transfer. Results from their flow visualization indicated that the bubble generation was suppressed by raising the mass flux and subcooling, and only the liquid subcooling showed significant effect on bubble size.

Based on the available experimental data from open literature, some correlating equations for subcooled flow boiling heat transfer have been proposed [10–12]. A general subcooled flow boiling correlation compared with a large amount of data from annuli was developed

by Shah [10]. The data include water, R-113, and methanol for heating of inner, outer, and both tubes of the annuli. Kandlikar [11] divided the subcooled flow boiling into the partial boiling, fully developed boiling and significant void flow regions. Meanwhile, appropriate correlations were presented to predict the heat transfer in each region. A flow boiling correlation based on an explicit nucleate boiling term rather than on an empirical boiling number dependence for vertical and horizontal flows in tubes and annuli was proposed by Gungor and Winterton [12].

It is well known that plate heat exchangers (PHEs) are commonly used in food processing, heating, chemical reaction processes and other industrial applications for many years. Particularly, the plate heat exchangers have been introduced recently to the refrigeration and air conditioning systems as evaporators or condensers for their high efficiency and compactness. The advantages of using PHEs were clearly indicated in the studies of Shah and Focke [13]. Unfortunately, most studies about PHEs reported in the open literature focused on single-phase liquid-to-liquid heat transfer [14–17]. The results from these studies indicated that the measured single-phase convection heat transfer coefficient was mainly affected by the chevron angle and surface area enlargement factor (ratio of the actual corrugated surface area to its projected area) of the plates. Recently, the frictional pressure drop in an air–water two-phase flow moving through plate heat exchangers was measured by Kreissig and Müller-Steinhagen [18] and Tribbe and Müller-Steinhagen [19,20]. The pressure drop was noted to increase linearly with the flow quality. Moreover, their flow visualization revealed five two-phase flow patterns in the PHE [20] similar to those observed in circular channels. To complement our previous studies on the phase change heat transfer in a plate heat exchanger [21,22], subcooled flow boiling of refrigerant R-134a in a plate heat exchanger is experimentally investigated in this study. Moreover, correlations will be developed for predicting the boiling heat transfer coefficient and bubble departure diameter. Besides, visualization of bubbles will be conducted to augment our fundamental understanding of the subcooled boiling heat transfer mechanism.

2. Experimental apparatus and procedures

The schematic of the experimental apparatus for the present study is depicted in Fig. 1. The experimental system consists of four independent loops and a data acquisition system. It includes a refrigerant loop, two water loops (one for the preheater and the other for the test section), and a cold water–glycol loop. To control

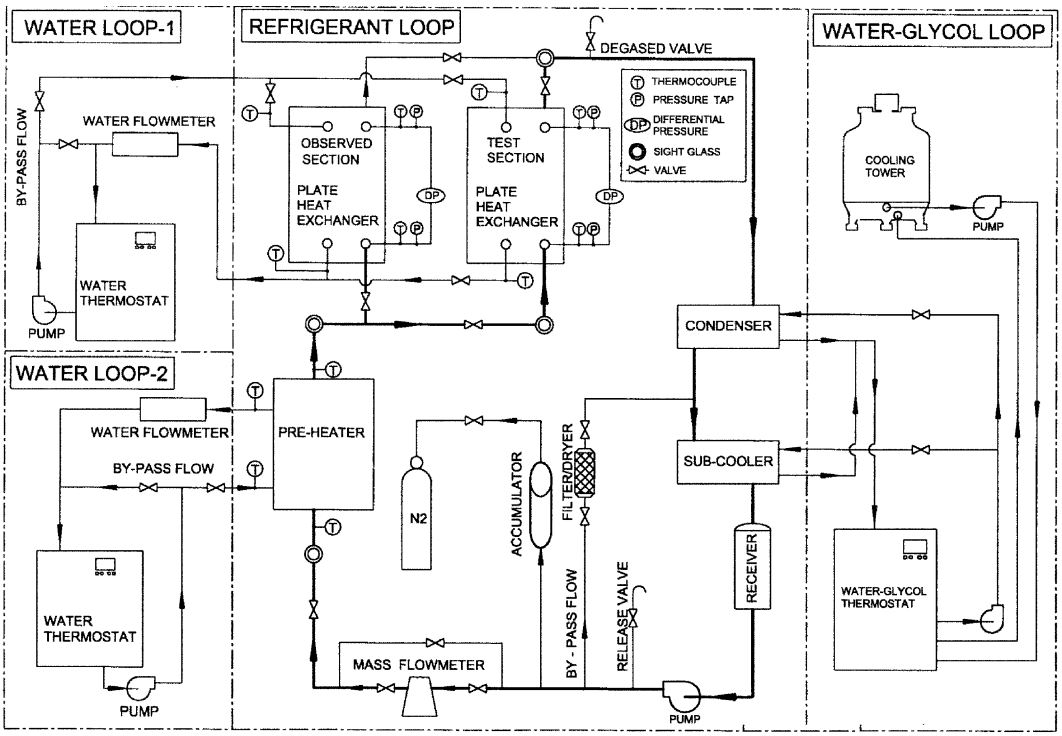

Fig. 1. Schematic diagram of the experimental system.

various test conditions of R-134a (including boiling heat flux, refrigerant mass flux, inlet subcooling and system pressure) in the test section, we need to control the temperature and flow rate in the other three loops.

2.1. Refrigerant loop

The refrigerant loop contains a variable-speed refrigerant pump that delivers the subcooled refrigerant to the preheater. The refrigerant mass flow rate is mainly controlled by an AC motor through the change of the inverter frequency. The flow rate can be further adjusted by regulating the bypass valve in the flow path from the refrigerant pump. To measure the refrigerant mass flow rate, an accurate mass flux meter is installed between the refrigerant pump and preheater with a reading accuracy of $\pm 1\%$. The subcooled refrigerant liquid is heated in the preheater to a prescribed inlet subcooling before entering the test section. Then, the subcooled liquid refrigerant moves into the test section and boils there. The refrigerant leaving the test section is condensed and subcooled by the low-temperature water–glycol in the shell-and-coil heat exchangers acting as the condenser and subcooler. An accumulator is connected to a high-pressure nitrogen tank to dampen the fluctuation of the flow rate and pressure. In addition, the loop is also equipped with a receiver, a filter/dryer, a release valve, a degassed valve and four sight glasses. The pressure of the refrigerant loop can be controlled by varying the temperature and flow rate of the water–glycol in the condenser and subcooler. Two absolute pressure transducers are installed at the inlet and exit of the test section with resolution up to ± 2 kPa. All the water and refrigerant temperatures are measured by Type T copper-constantan thermocouples with a calibrated accuracy of ± 0.2 °C. A polyethylene insulation layer of 5 cm thickness is wrapped around the whole loop to reduce the heat loss from the ambient.

2.2. Test section

The test section for the subcooled flow boiling study conducted here consists of two plate heat exchangers, one for flow visualization and the other for measuring heat transfer data. The plate heat exchanger for collecting the boiling data is formed by three commercial SS-316 plates manufactured by Kaori Heat Treatment, Taiwan. The plate surfaces are pressed to become grooved with a corrugated sinusoidal shape and 60° chevron angle, which is the angle of V-grooves to the vertical axis of the plate. The detailed geometry data of the plate heat exchanger are given in Fig. 2. The corrugated grooves on the right and left outer plates have a V shape but those in the middle plate have an inverted V shape on both sides. This arrangement allows the flow stream to be divided into two different flow directions

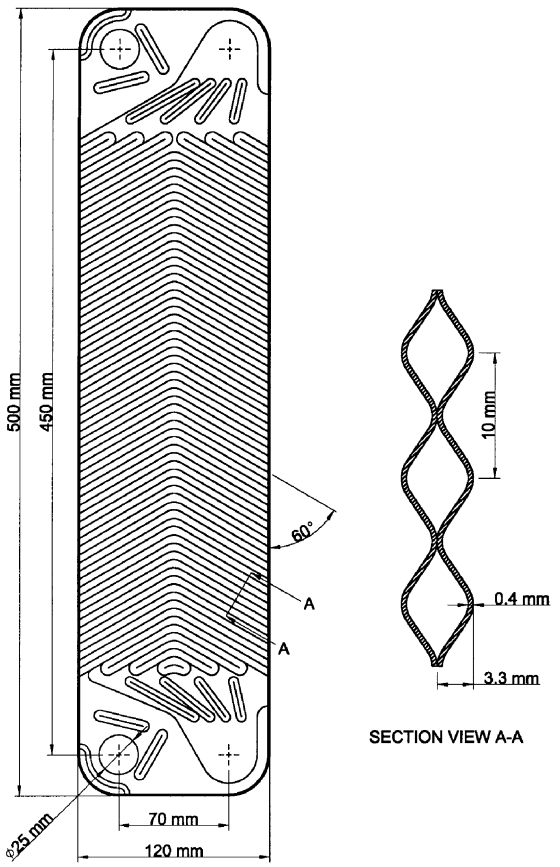

Fig. 2. Schematic diagram of plate heat exchanger.

along the plates. Thus, the flow moves mainly along the grooves in each plate. Due to the inverted V shapes between two neighbor plates the flow streams near the two plates cross each other in each channel. This cross-flow results in significant flow unsteadiness and randomness. In fact, the flow is highly turbulent even when the Reynolds number is low. For conformity, the plate heat exchanger for visualization is chosen to have the same structure as that described above for the data collection except that the right outer plate is made of transparent acrylic, which is machined and then polished to the same geometry. In each plate heat exchanger two vertical counterflow channels are formed by three plates. Upflow of refrigerant R-134a in one channel is heated by the downflow of hot water in the other channel. The heat transfer rate in the test section is calculated by measuring the water temperature drop between the water channel inlet and outlet and by measuring the water flow rate.

2.3. Water loop for test section

The water loop in the experimental system for circulating the hot water through the test section contains a

20 l water thermostat with a 0.5 kW heater, and a water pump is used to drive the hot water at a specified water flow rate. A bypass valve can also be used to adjust the water flow rate. The accuracy of measuring the water flow rate is ±0.5%.

2.4. Water loop for preheater

Another water loop designed for the preheater consists of a 125 l hot water thermostat, and the hot water at specified temperature and flow rate is driven by a water pump to the preheater. Similarly, a bypass valve is also used to adjust the flow rate.

2.5. Water–glycol loop

Both the condenser and subcooler, which respectively condense and subcool the refrigerant R-134a leaving the test section, are cooled by an independent low-temperature water–glycol loop. The cooling capacity is 3.5 kW for the water–glycol at −20 °C. A 0.5 hp pump is used to drive the water–glycol at a specified flow rate to the condenser as well as to the subcooler. A bypass valve is also provided to adjust the flow rate.

2.6. Data acquisition

The data acquisition unit includes a recorder, a 24 V–3 A power supply, and a controller. The water flowmeter and differential pressure transducer need the power supply as a driver to output an electric current of 4–20 mA. The data signals are collected and converted in the data acquisition unit (Hybrid recorder). The converted signals are then transmitted to a host computer through a GPIB interface for further calculation.

2.7. Experimental procedures

In each test the R-134a pressure at the test section inlet is first maintained at a specified level by adjusting the temperature and flow rate of the water–glycol moving through the condenser and subcooler. Then, the temperature and flow rate of the hot water loop for the preheater are adjusted to keep the R-134a at the desired inlet subcooling state. Next, the heat transfer rate between the counterflow channels in the test section can be varied by changing the water temperature and flow rate in the water loop for the test section. Meanwhile, by selecting the frequency of the inverter connecting to the refrigerant pump and by adjusting the bypass valve, the R-134a flow rate in the test section is maintained at a desired value.

In the test any changes of the system variables will lead to fluctuations in the temperature and pressure of the refrigerant flow. It takes about 20–100 min for the system to reach a statistically stable state at which the variations of the time-averaged inlet and outlet temperatures are both less than ±0.2 °C, and the variations of the pressure and imposed heat flux are within 1% and 4%, respectively. Then the data acquisition unit is initiated to scan all the data channels 10 times in 50 s. The mean value of the data for each channel is used to calculate the boiling heat transfer coefficient and pressure drop. Additionally, the flow rate of water in the test section should be high enough to have turbulent flow in the water side so that the associated single-phase heat transfer in it is high enough for balancing the boiling heat transfer in the refrigerant side. In this study, the Reynolds number of the water flow is maintained beyond 200.

2.8. Uncertainty analysis

The uncertainties of the experimental results are analyzed by the procedures proposed by Kline and McClintock [23]. The detailed results from the present uncertainty analysis for the experiments conducted here are summarized in Table 1. It was noted in the uncertainty analysis that the uncertainty associated with the heat transfer area for the subcooled boiling, which is estimated from flow visualization, is the main uncertainty source in evaluating the subcooled boiling heat transfer coefficient.

3. Data reduction

A data reduction analysis is needed in the present measurement to deduce the heat transfer rate from the

Table 1
Summary of the uncertainty analysis

Parameter	Uncertainty
PHE geometry	
Length, width and thickness (m)	±0.00005
Area of the plate (m^2)	$\pm 7 \times 10^{-5}$
Parameter measurement	
Temperature, T (°C)	±0.2
Temperature difference, ΔT (%)	±4.5%
System pressure, P (MPa)	±0.002
Pressure drop, ΔP (Pa)	±200
Water flow rate, W_w (%)	±2
Mass flux of refrigerant, G (%)	±2
Single-phase heat transfer	
Heat transfer rate, Q (%)	±6.5
Heat transfer coefficient, h_w (%)	±8.5
Heat transfer coefficient, $h_{r,l}$ (%)	±11
Subcooled flow boiling heat transfer	
Boiling heat flux, q (%)	±10.5
Heat transfer coefficient, $h_{r,sub}$ (%)	±19.7

water to the refrigerant in the test section. From the definition of the hydraulic diameter, Shah and Focke [13] suggested the use of two times the mean channel spacing as the hydraulic diameter for the plate heat exchanger when the channel width is much larger than the channel spacing.

The subcooled flow boiling heat transfer coefficient is calculated by reducing the measured raw data in a computer program. The reduction procedures are given in the following.

In the initial water-to-refrigerant single-phase heat transfer tests for R-134a in the plate heat exchanger, the physical properties of water and R-134a were calculated according to the averages of the inlet and outlet bulk fluid temperatures. The heat transfer rate between the hot water and refrigerant sides in the test section was obtained from the measured flow rate and total temperature drop in the water side, that is,

$$Q_{\mathrm{w}} = W_{\mathrm{w}} C_{p,\mathrm{w}} (T_{\mathrm{w,i}} - T_{\mathrm{w,o}}), \tag{1}$$

in which W_{w} and $C_{p,\mathrm{w}}$ are the flow rate and specific heat of water, respectively. The overall heat transfer coefficient between the two counter channel flows was then calculated from

$$U = \frac{Q_{\mathrm{w}}}{A\,\mathrm{LMTD}}, \tag{2}$$

where A is the heat transfer area accounting for the actual corrugated surface of the plate. For the present PHE the area enlargement factor is 1.29. The log mean temperature difference (LMTD) is determined from

$$\mathrm{LMTD} = \frac{(\Delta T_1 - \Delta T_2)}{\ln(\Delta T_1/\Delta T_2)}, \tag{3}$$

with

$$\begin{aligned} \Delta T_1 &= T_{\mathrm{w,i}} - T_{\mathrm{r,o}}, \\ \Delta T_2 &= T_{\mathrm{w,o}} - T_{\mathrm{r,i}}. \end{aligned} \tag{4}$$

In view of the same heat transfer area in the refrigerant and water sides, the relation between the overall heat transfer coefficient and convection heat transfer coefficient of liquid R-134a is

$$\frac{1}{h_{\mathrm{r,l}}} = \frac{1}{U} - \frac{1}{h_{\mathrm{w}}} - R_{\mathrm{wall}} A, \tag{5}$$

where $h_{\mathrm{r,l}}$ and h_{w} are respectively the heat transfer coefficients for single-phase refrigerant R-134a and water flows, and $R_{\mathrm{wall}}A$ is the wall thermal resistance. To obtain the single-phase R-134a heat transfer coefficient, the heat transfer coefficient for the water flow needs to be determined first. This is accomplished by means of separate single-phase water-to-water tests on the same apparatus. The subsequent Wilson-plot analyses of the measured data yield the individual heat transfer coefficients between the channels.

How the subcooled flow boiling heat transfer coefficient of the refrigerant flow is obtained from the measured raw data is described next. Firstly, the total heat transfer rate between the counterflows in the plate heat exchanger Q_{w} is calculated from the hot water side. Note that boiling does not prevail over the entire plate surface in the refrigerant side for the subcooled liquid R-134a entering the test section. In fact, in the entry portion of the refrigerant channel heat transfer takes place in the single-phase liquid R-134a flow. Beyond this single-phase region boiling occurs and dominates the heat transfer processes. Hence the overall heat transfer coefficient for the subcooled boiling region is calculated from

$$U_{\mathrm{sub}} = \frac{Q_{\mathrm{w,sub}}}{A_{\mathrm{sub}}\,\mathrm{LMTD}}. \tag{6}$$

Here A_{sub} is the area of the plate surface on which boiling occurs. It is estimated from the flow visualization. $Q_{\mathrm{w,sub}}$ is the subcooled boiling heat transfer rate calculated by subtracting the single-phase heat transfer rate $Q_{\mathrm{w,single}}$ from the total heat transfer rate Q_{w},

$$Q_{\mathrm{w,sub}} = Q_{\mathrm{w}} - Q_{\mathrm{w,single}}. \tag{7}$$

The LMTD is again determined from

$$\mathrm{LMTD} = \frac{(\Delta T_1 - \Delta T_2)}{\ln(\Delta T_1/\Delta T_2)}, \tag{8}$$

but for the subcooled boiling

$$\begin{aligned} \Delta T_1 &= T_{\mathrm{w,i}} - T_{\mathrm{r,o}}, \\ \Delta T_2 &= T_{\mathrm{w,b}} - T_{\mathrm{r,b}}, \end{aligned} \tag{9}$$

where $T_{\mathrm{r,b}}$ and $T_{\mathrm{w,b}}$ are respectively the temperatures of the refrigerant and hot water at the locations where R-134a starts to boil in the PHE, as indicated schematically in Fig. 3. The relation between $T_{\mathrm{r,b}}$ and $T_{\mathrm{w,b}}$ can be calculated according to the energy balance of the two counterflows in the single-phase heat transfer region. Note that in the single-phase region

$$Q_{\mathrm{w,single}} = W_{\mathrm{w}} C_{p,\mathrm{w}} (T_{\mathrm{w,b}} - T_{\mathrm{w,o}}) = W_{\mathrm{r}} C_{p,\mathrm{r}} (T_{\mathrm{r,b}} - T_{\mathrm{r,i}}). \tag{10}$$

We also have

$$Q_{\mathrm{w,single}} = Q_{\mathrm{r,single}} = U_{\mathrm{single}} A_{\mathrm{single}}\,\mathrm{LMTD}_{\mathrm{single}}, \tag{11}$$

where $\mathrm{LMTD}_{\mathrm{single}}$ and U_{single} are evaluated from the equations

$$\mathrm{LMTD}_{\mathrm{single}} = \frac{(T_{\mathrm{w,b}} - T_{\mathrm{r,b}}) - (T_{\mathrm{w,o}} - T_{\mathrm{r,i}})}{\ln[(T_{\mathrm{w,b}} - T_{\mathrm{r,b}})/(T_{\mathrm{w,o}} - T_{\mathrm{r,i}})]} \tag{12}$$

and

$$\frac{1}{U_{\mathrm{single}}} = \frac{1}{h_{\mathrm{r,l}}} + \frac{1}{h_{\mathrm{w}}} + R_{\mathrm{wall}} A_{\mathrm{single}}. \tag{13}$$

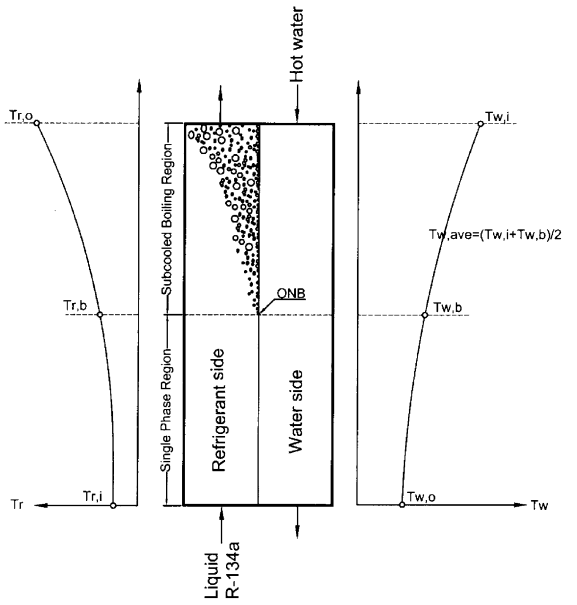

Fig. 3. Sketch of the counterflow channels showing the temperatures of the refrigerant and water at the inlets and outlets and incipient boiling in each channel.

With the data for $h_{r,l}$ and h_w measured before the two-phase experiment, Eqs. (10) and (11) can be solved simultaneously for $T_{w,b}$ and $T_{r,b}$ by numerical iteration. Finally, the subcooled flow boiling heat transfer coefficient in the flow of R-134a is evaluated from the equation

$$\frac{1}{h_{r,sub}} = \frac{1}{U_{sub}} - \frac{1}{h_w} - R_{wall}A_{sub}. \quad (14)$$

4. Results and discussion

In the present study of the subcooled flow boiling heat transfer of R-134a and the associated bubble characteristics in the plate heat exchanger, the refrigerant mass flux G is varied from 50 to 200 kg/m^2 s, boiling heat flux q from 0 to 35 kW/m^2, liquid inlet subcooling ΔT_{sub} from 10 to 15 °C for the system pressure at 0.6 and 0.7 MPa (R-134a saturation temperature T_{sat} at 21.6 and 26.7 °C). In what follows the characteristics of the subcooled boiling heat transfer are illustrated by presenting the boiling curves, which show the variations of the boiling heat flux q with the cross-channel superheat $(T_{w,ave} - T_{sat})$ for various cases. In view of the fact that the plate surface temperature is not measured in this study, the cross-channel superheat instead of the wall superheat is chosen to present our boiling data. Effects of the refrigerant mass flux, boiling heat flux, inlet subcooling and system pressure (saturation temperature) on the heat transfer data will be examined in detail. In addition, the characteristics of the bubbles during the boiling processes on the plate surface will be discussed according to the results from the flow visualization.

4.1. Subcooled flow boiling curves

Effects of the refrigerant mass flux on the subcooled flow boiling heat transfer are manifested in Fig. 4 for different inlet subcoolings ($\Delta T_{sub} = 10$ and 15 °C). An inspection of a given boiling curve for a fixed refrigerant mass flux reveals that, as the heat flux at the plate between the water and refrigerant channels is raised gradually from an unheated state by raising the temperature of the hot water side, an almost linear rise in the cross-channel superheat results. This suggests that at a small q no boiling takes place in the refrigerant R-134a flow and the heat transfer in it is due to single-phase forced convection. It is of interest to note that this single-phase heat transfer region in the refrigerant side extends significantly to the average water side temperature $T_{w,ave}$ well above the saturation temperature of the refrigerant T_{sat}. The cross-channel superheat, $T_{w,ave} - T_{sat}$, can be as high as 10 °C for $G = 50$ kg/m^2 s with $\Delta T_{sub} = 15$ °C and $T_{sat} = 26.7$ °C (Fig. 4(a)) with no boiling on the plate surface in the R-134a channel. It is further noted that a sharp rise in the boiling heat flux appears at a certain high cross-channel superheat, obviously due to the sudden appearance of the boiling on the plate surface. Thus, we have onset of nucleate boiling (ONB) at this superheat. Note that for higher mass fluxes of $G = 100$ and 200 kg/m^{2}s the cross-channel superheats at ONB are slightly smaller and the sudden jump in the heat flux at ONB is not observed. Furthermore, the temperature undershoot during ONB is rather small in the subcooled flow boiling for the PHE according to the present data, unlike that in the annular duct [9]. Beyond ONB, the increase in the boiling heat flux with the superheat is much larger than that in the single-phase region, as evident from the much steeper slope in the boiling curves. Besides, the boiling heat flux is higher for a higher mass flux. At a smaller liquid subcooling the incipient boiling occurs at a smaller superheat and the jump in q at ONB is also smaller, as is clear from comparing the results in Fig. 4(a) with those in Fig. 4(b).

Next, the hysteresis in the boiling curves is illustrated in Fig. 5 for $G = 50$ and 200 kg/m^2, $T_{sat} = 26.7$ °C and $\Delta T_{sub} = 15$ °C. The results for $G = 50$ kg/m^2 s indicate that when the cross-channel superheat is lowered gradually from a high level at which the boiling on the plate surface is rather intense, the nucleate boiling can be maintained at a very low superheat. We have boiling even at a superheat of 3 °C (Fig. 5(a)) and the hysteresis during the flow boiling can be clearly seen. However, at the higher G of 200 kg/m^2 s the hysteresis is very slight

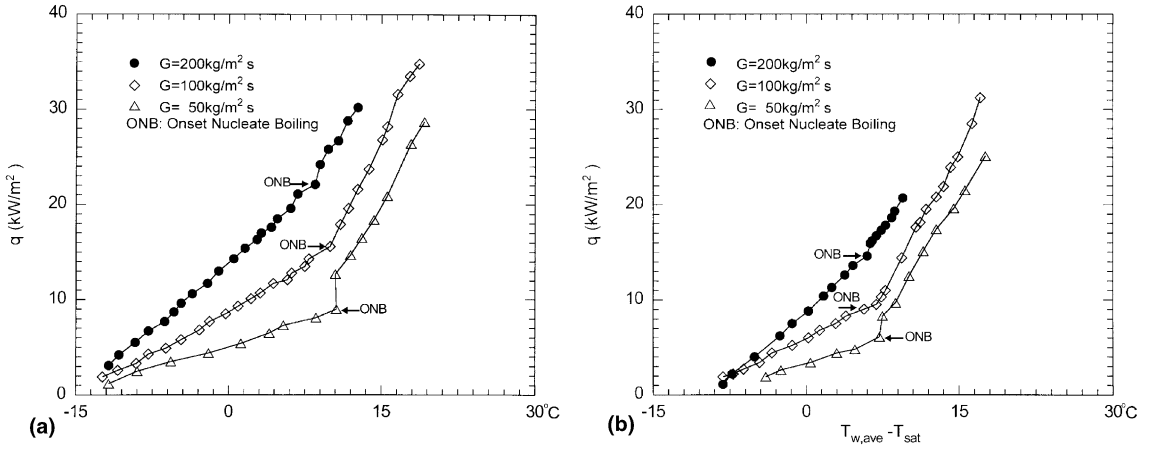

Fig. 4. Boiling curves for various mass fluxes ($G = 50$, 100 and 200 kg/m^2 s) and $T_{sat} = 26.7$ °C at $\Delta T_{sub} =$ (a) 15 °C and (b) 10 °C.

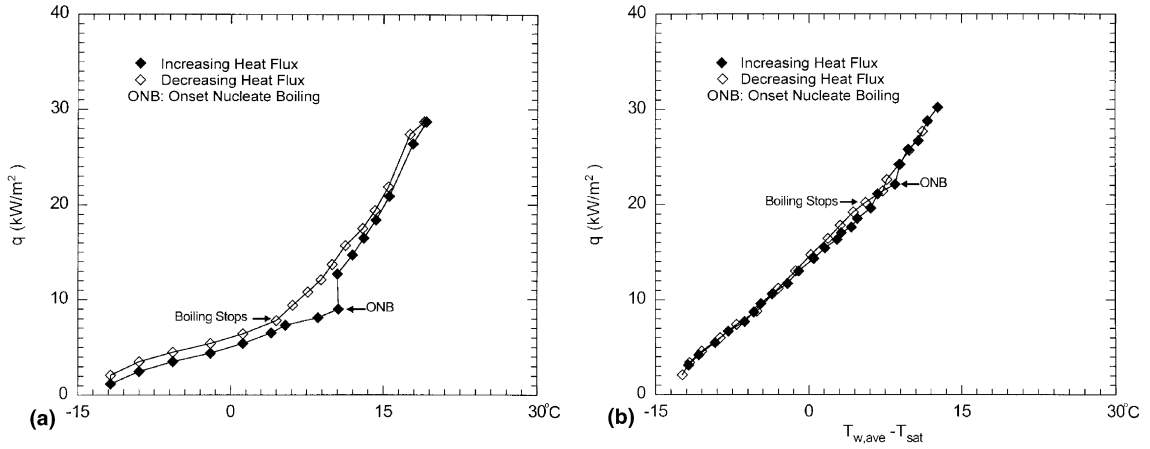

Fig. 5. Boiling curves showing the degree of the hysteresis for $\Delta T_{sub} = 15$ °C and $T_{sat} = 26.7$ °C at $G =$ (a) 50 kg/m^2 s and (b) 200 kg/m^2 s.

(Fig. 5(b)). These trends are in agreement with those noted by Hasan et al. [2] that the boiling hysteresis is less severe at a higher flow velocity.

Then, the subcooled flow boiling curves for two different saturation temperatures with $T_{sat} = 21.6$ and 26.7 °C are shown in Fig. 6 for $G = 100$ kg/m^2 s and $\Delta T_{sub} =$ 10 and 15 °C. The results indicate that the boiling heat flux at a given cross-channel superheat is much larger for a higher T_{sat} for both liquid subcoolings. This exhibits that an increase in the saturation temperature of the refrigerant results in better heat transfer. But in the single-phase region before ONB the saturation temperature shows negligible effects on the heat transfer in the refrigerant flow. This is attributed to the relatively small change of the physical properties of the liquid R-134a with its saturation temperature.

Finally, the effects of the subcooling are shown in Fig. 7 for $\Delta T_{sub} = 10$ and 15 °C at $G = 100$ kg/m^2 s and $T_{sat} = 21.6$ and 26.7 °C. The results indicate that the boiling heat flux is higher for a higher subcooling in the single-phase heat transfer region. But in the nucleate boiling region the difference in the boiling heat fluxes for $\Delta T_{sub} = 10$ and 15 °C is rather small. It is further noted that at a larger liquid subcooling the cross-channel superheat needed to initiate the nucleate boiling and the corresponding boiling heat flux are also slightly higher.

4.2. Subcooled flow boiling heat transfer coefficient

The variations of the subcooled flow boiling heat transfer coefficient with the boiling heat flux are shown in Fig. 8 at two different mass fluxes (150 and 100

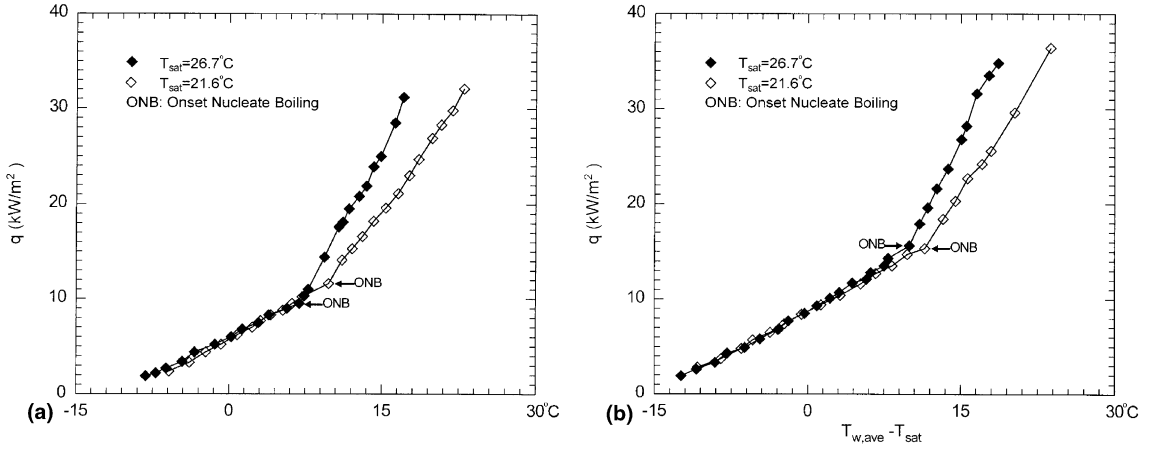

Fig. 6. Boiling curves for various saturation temperatures (T_{sat} = 21.6 and 26.7 °C) and G = 100 kg/m^2 s at ΔT_{sub} = (a) 10 °C and (b) 15 °C.

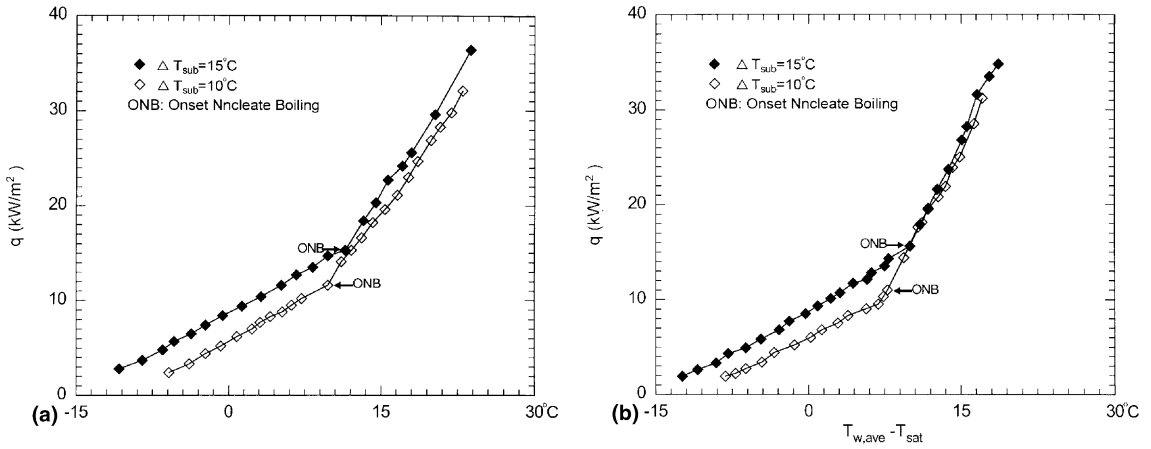

Fig. 7. Boiling curves for various inlet subcoolings (ΔT_{sub} = 10 and 15 °C) and G = 100 kg/m^2 s at T_{sat} = (a) 21.6 °C and (b) 26.7 °C.

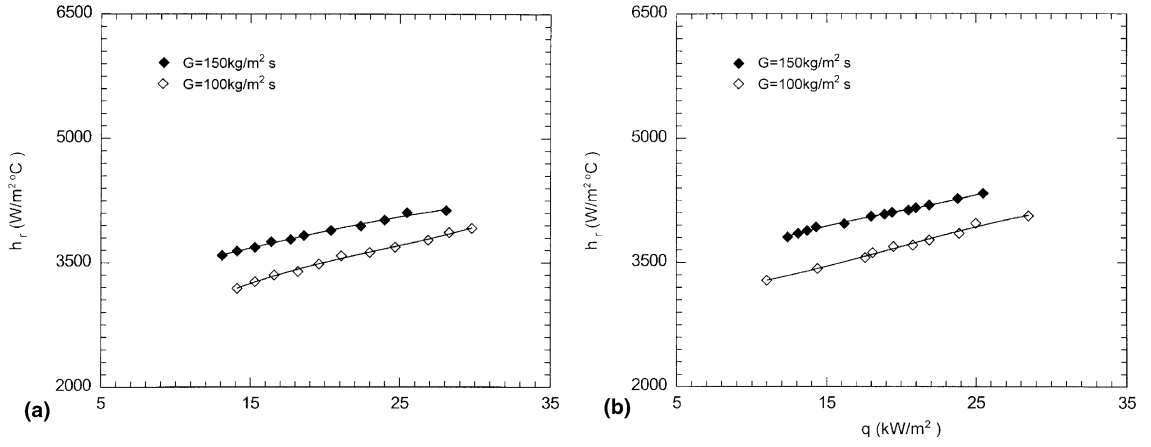

Fig. 8. Variations of the subcooled boiling heat transfer coefficient with the boiling heat flux for the various mass fluxes (G = 100 and 150 kg/m^2 s) and ΔT_{sub} = 10 °C at T_{sat} = (a) 21.6 °C and (b) 26.7 °C.

kg/m^2 s) for $\Delta T_{sub} = 10$ °C and $T_{sat} = 21.6$ and 26.7 °C. The results indicate that at a given mass flux the boiling heat transfer coefficient increases slightly with the heat flux. But a rise in the mass flux produces a noticeable increase in the boiling heat transfer rate. Specifically, for a higher mass flux of 150 kg/m^{2}s the heat transfer coefficient is about 10% on average higher than that of 100 kg/m^2 s.

Next, the effects of the saturation temperature on the subcooled boiling heat transfer coefficient are examined. Fig. 9 presents the data for the boiling heat transfer coefficient at the mass flux of 100 kg/m^{2}s for two different saturation temperatures of $T_{sat} = 21.6$ and 26.7 °C. The results indicate that an increase in the saturation temperature leads to a slight improvement in the boiling heat transfer.

Finally, the effects of the inlet subcooling are shown in Fig. 10 for $\Delta T_{sub} = 10$ and 15 °C at $G = 150$ kg/m^2 s and $T_{sat} = 21.6$ and 26.7 °C. The results suggest that the boiling heat transfer coefficient is slightly higher for a larger subcooling.

4.3. Bubble characteristics

Figs. 11 and 12 show the typical flow photos of the bubbles in the subcooled flow boiling taken at the same selected area on the plate surface for various boiling heat fluxes at $G = 50$ kg/m^2 s, $T_{sat} = 26.7$ °C and $\Delta T_{sub} = 10$ and 15 °C. The results indicate that at a higher heat flux q a larger fraction of the plate surface is covered by the bubbles, suggesting that more nucleation sites on the plate are activated for a higher q. Besides, the bubble

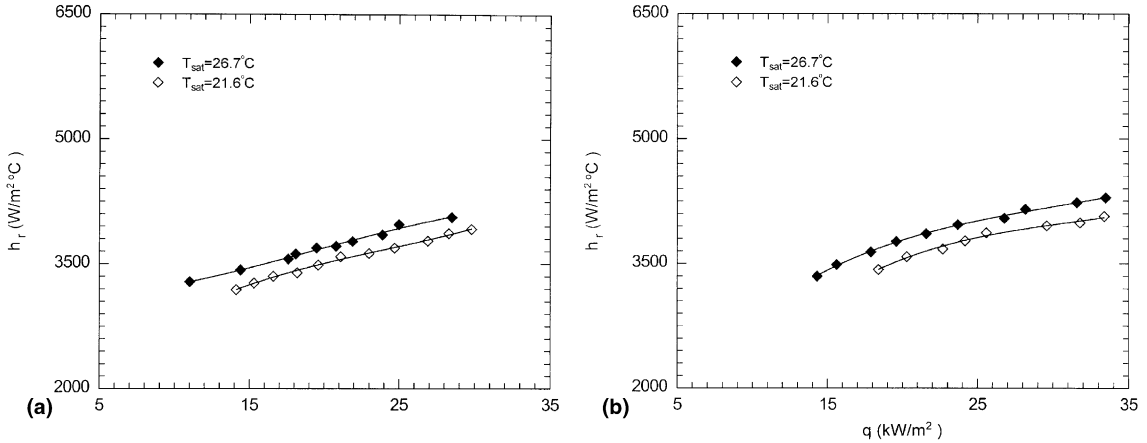

Fig. 9. Variations of the subcooled boiling heat transfer coefficient with the boiling heat flux for the various saturated temperatures ($T_{sat} = 21.6$ and 26.7 °C) and $G = 100$ kg/m^2 s at ΔT_{sub} = (a) 10 °C and (b) 15 °C.

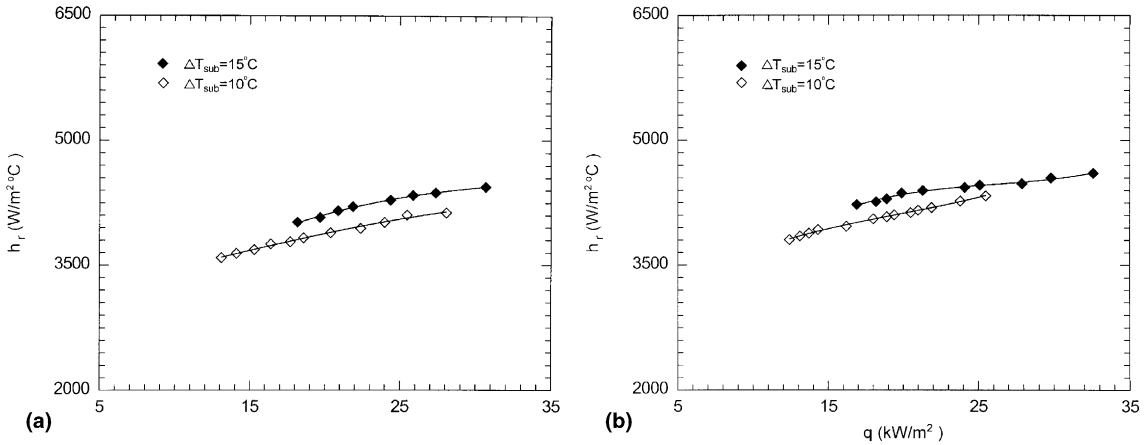

Fig. 10. Variations of the subcooled boiling heat transfer coefficient with the boiling heat flux for the various inlet temperatures ($\Delta T_{sub} = 10$ and 15 °C) and $G = 150$ kg/m^2 s at T_{sat} = (a) 21.6 °C and (b) 26.7 °C.

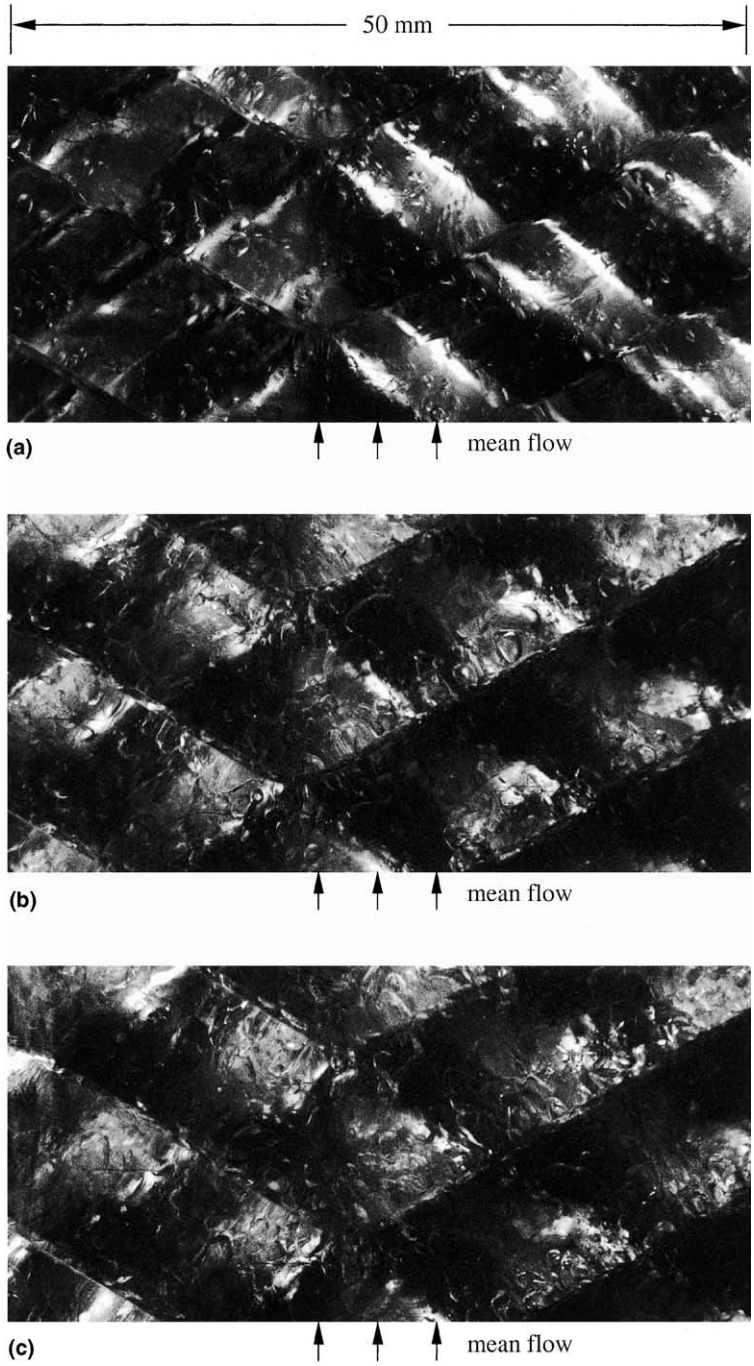

Fig. 11. Photos for the subcooled flow boiling of R-134a at $G = 50$ kg/m^2 s, $T_{sat} = 26.7$ °C and $\Delta T_{sub} = 10$ °C for $q =$ (a) 6 kW/m^2, (b) 10 kW/m^2 and (c) 15 kW/m^2.

generation frequency and the bubble rising velocity in the liquid were found to be also higher. Thus, the corresponding boiling heat transfer from the surface is better. A close inspection of the photos reveals that the average diameter of bubbles about to depart from the plate surface (d_p) changes significantly with the heat flux and it ranges approximately from 0.4 to 0.7 mm, which is rather small in comparison with that in boiling of water. Moreover, at a high q a large number of bubbles are generated from the surface and these bubbles tend to

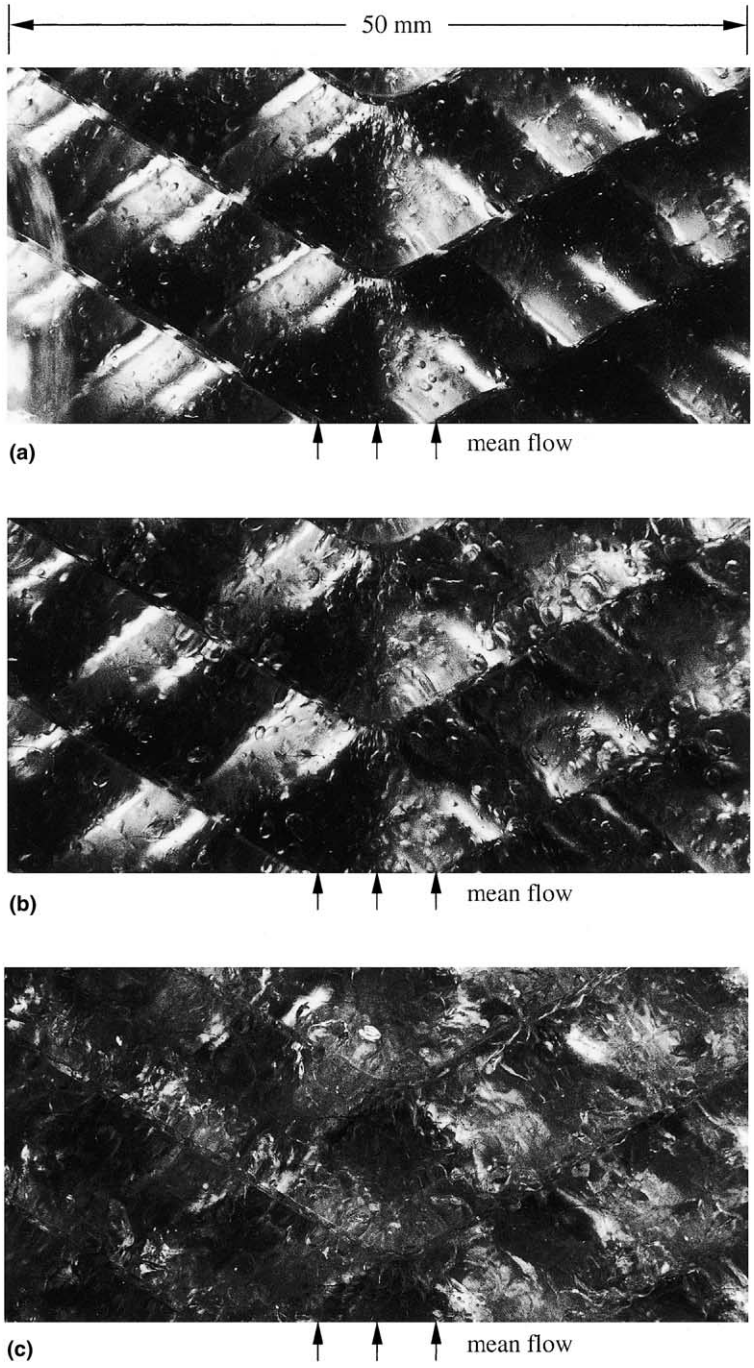

Fig. 12. Photos for the subcooled flow boiling of R-134a at $G = 50$ kg/m^2 s, $T_{sat} = 26.7$ °C and $\Delta T_{sub} = 15$ °C for $q =$ (a) 8.5 kW/m^2, (b) 15 kW/m^2 and (c) 20 kW/m^2.

coalesce to form large bubbles, which are in vigorous agitating motion in the flow (Figs. 11(c) and 12(c)).

The photos for various refrigerant mass fluxes shown in Fig. 13 suggest that at a lower mass flux more bubbles are generated from a larger number of active nucleation sites. This is mainly attributed to the fact that at a constant heat flux q, the refrigerant flow and hence the plate surface are heated to higher temperatures for a lower G. Obviously, the higher refrigerant and plate temperatures at the lower refrigerant mass flux are fa-

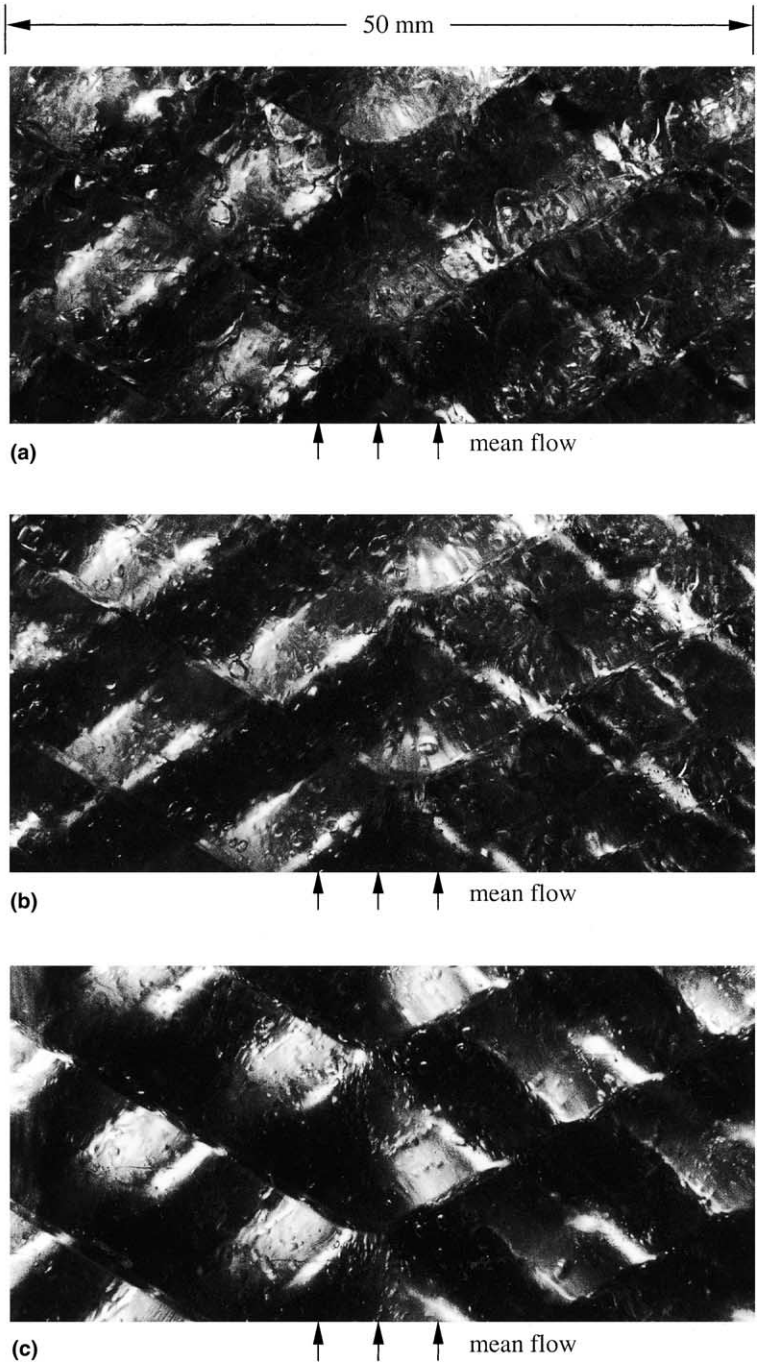

Fig. 13. Photos for the subcooled flow boiling of R-134a at $q = 15$ kW/m^2, $T_{sat} = 26.7$ °C and $\Delta T_{sub} = 10$ °C for $G =$ (a) 50 kg/m^2 s, (b) 75 kg/m^2 s and (c) 100 kg/m^2 s.

vorable for enhancing the boiling heat transfer from the surface. But we also note that at a higher refrigerant mass flux the liquid R-134a flow can quickly sweep the bubbles away from the grooved surface and hence causes significant increase in boiling heat transfer. The above two opposite effects coexist for a change in the refrigerant mass flux. Moreover, the size of the bubbles about to depart from the plate surface is affected by the mass flux to a noticeable degree. For example, the bubble size for $G = 100$ kg/m^2 s is about 40–50%

smaller than that for $G = 50$ kg/m^2 s. Then, at the higher saturation temperature the bubbles were noted to be in slightly stronger agitating motion.

Finally, the bubble characteristics affected by the inlet subcooling are illustrated in Fig. 14 by showing the photos for three different subcoolings at $G = 50$ kg/m^2 s, $T_{sat} = 26.7$ °C and $q = 11.5$ kW/m^2. Note that at the same G, T_{sat} and q the plate temperature is lower for a higher liquid subcooling. Besides, in a highly subcooled liquid the bubbles are significantly suppressed and grow

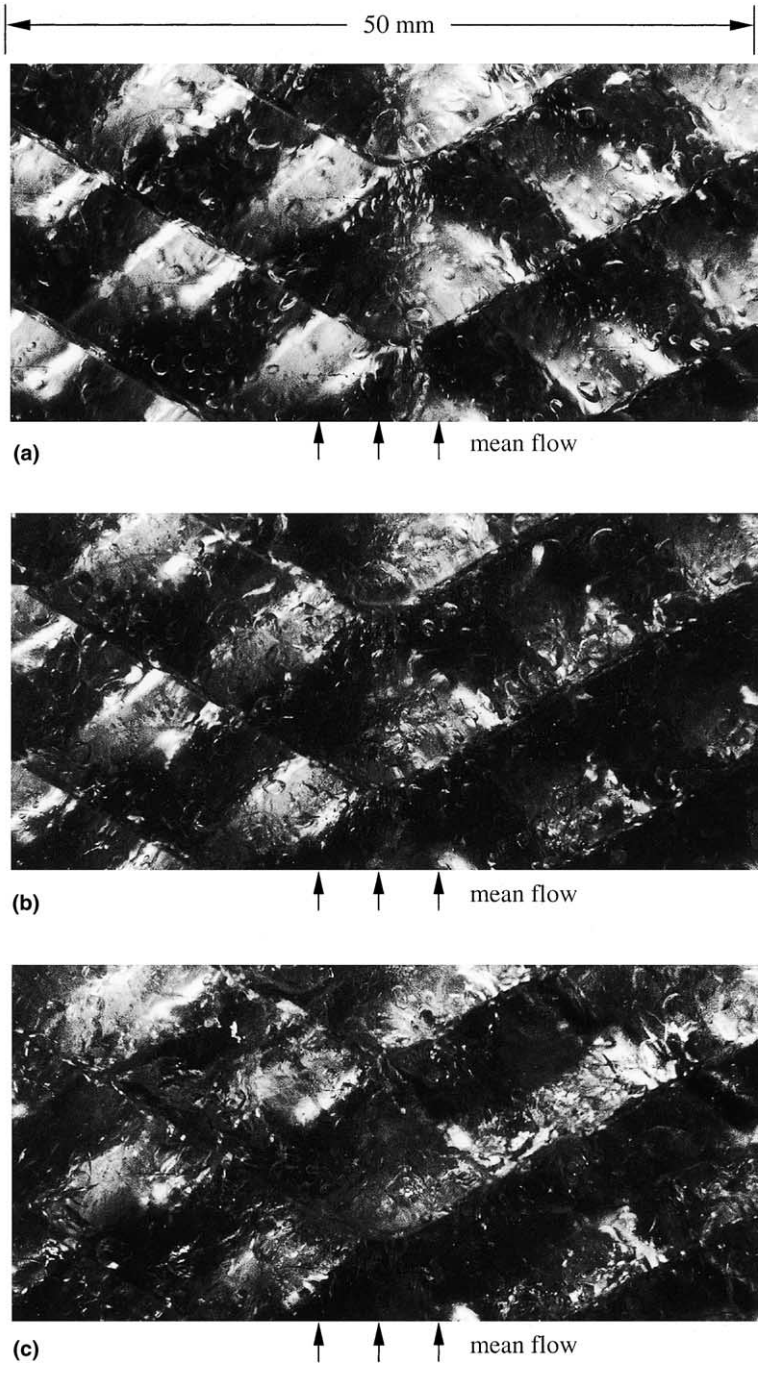

Fig. 14. Photos for the subcooled flow boiling of R-134a at $G = 50$ kg/m^2 s, $T_{sat} = 26.7$ °C and $q = 11.5$ kW/m^2 for $\Delta T_{sub} =$ (a) 15 °C, (b) 10 °C and (c) 0 °C.

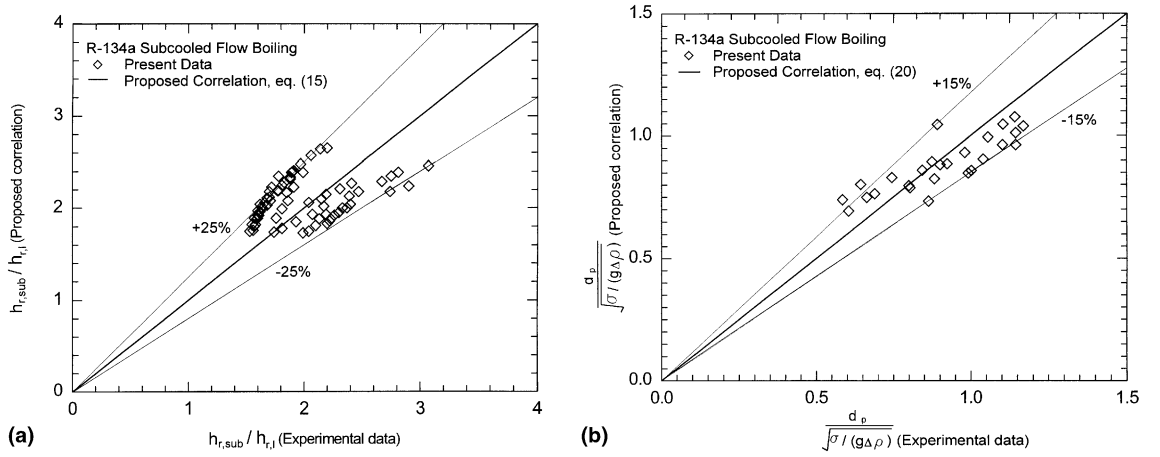

Fig. 15. Comparison of the proposed correlations with the present data for (a) the heat transfer coefficient and (b) the bubble departure diameter in the subcooled flow boiling.

slowly. Thus, the bubbles are smaller ($d_p = 0.4$ mm) and discrete at $\Delta T_{sub} = 15$ °C (Fig. 14(a)) as compared to $\Delta T_{sub} = 10$ and 0 °C. Furthermore, at smaller ΔT_{sub} of 10 and 0 °C the plate temperature is higher, more bubbles coalesce and the bubbles are in vigorous motion (Figs. 14(b) and (c)).

4.4. Correlation equations

According to the present experimental data, the heat transfer coefficient in the subcooled flow boiling of R-134a in the PHE can be correlated as

$$h_{r,sub} = h_{r,l}[1.2Fr^{0.75} + 13.5Bo^{1/3}Ja^{1/4}]. \quad (15)$$

Here Fr, Bo and Ja are respectively the Froude, boiling and Jakob numbers, defined as

$$Fr = \frac{G^2}{\rho_l^2 g D_h}, \quad (16)$$

$$Bo = \frac{q}{G i_{fg}} \quad (17)$$

and

$$Ja = \frac{\rho_l C_p \Delta T_{sat}}{\rho_g i_{fg}}. \quad (18)$$

Note that the convective effects of the flow boiling are explicitly expressed in the Froude number. Here, $h_{r,l}$ is determined from the empirical correlation of the data from the single-phase heat transfer tests as

$$h_{r,l} = 0.2092\left(\frac{k_l}{D_h}\right)Re^{0.78}Pr^{1/3}\left(\frac{\mu_{ave}}{\mu_{wall}}\right)^{0.14}. \quad (19)$$

The present data of the single-phase convection heat transfer coefficient are in good agreement with those calculated from the correlation proposed by Muley and Manglik [14]. Moreover, the proposed equation for subcooled flow boiling heat transfer coefficient (Eq. (15)) well correlates the present data with an average deviation of 8.6% (Fig. 15(a)).

Then, an empirical correlation for the average bubble departure diameter modified from that of Zeitoun and Shoukri [24] for the subcooled upward flow boiling in a vertical annular channel is proposed here to fit our data. It is

$$\frac{d_p}{\sqrt{\sigma/g\Delta\rho}} = \frac{0.93(\rho_l/\rho_g)^{1.23}}{Re^{0.35}[Ja + 165(\rho_l/\rho_g)^{1.23}/Bo^{0.487}Re^{1.58}]}. \quad (20)$$

This new correlation fits well with the present data with an average deviation of 12.8%, as shown in Fig. 15(b).

5. Concluding remarks

Experiments have been carried out in the present study to explore the subcooled flow boiling heat transfer and the associated bubble characteristics of R-134a in a plate heat exchanger. The major results can be summarized in the following.

1. For the subcooled flow boiling of R-134a in the PHE, the refrigerant mass flux and saturated temperature show significant influence on the boiling curves. The boiling hysteresis is important only at low refrigerant mass flux.
2. The subcooled boiling heat transfer coefficient is substantially affected by the refrigerant mass flux. But increases in the saturation temperature and inlet subcooling of the refrigerant only result in a slight improvement in the heat transfer.

3. Visualization of the boiling processes reveals that the bubbles are somewhat suppressed by raising the refrigerant mass flux and inlet subcooling. Moreover, the boiling heat flux and inlet subcooling show large effects on the bubble population, coalesce and generation frequency.

Acknowledgements

The financial support of this study by the engineering division of National Science Council of Taiwan, ROC, through the contract NSC 85-2221-E-009-06 is greatly appreciated.

References

[1] H. Müller-Steinhagen, A.P. Watkinson, N. Epstein, Subcooled-boiling and convective heat transfer to heptanes flowing inside an annulus and past a coiled wire: part I – experimental results, ASME J. Heat Transfer 108 (1986) 922–927.

[2] A. Hasan, R.P. Roy, S.P. Kalra, Experiments on subcooled flow boiling heat transfer in a vertical annular channel, Int. J. Heat Mass Transfer 33 (1990) 2285–2293.

[3] P. Sivagnanam, A.R. Balakrishnan, Y.B.G. Varma, On the mechanism of subcooled flow boiling of binary mixtures, Int. J. Heat Mass Transfer 37 (1994) 681–689.

[4] V.H. Del Valle M, D.B.R. Kenning, Subcooled flow boiling at high heat flux, Int. J. Heat Mass Transfer 28 (1985) 1907–1920.

[5] J.F. Klausner, R. Mei, D.M. Bernhard, L.Z. Zeng, Vapor bubble departure in forced convection boiling, Int. J. Heat Mass Transfer 36 (1993) 651–662.

[6] L.H. Chien, R.L. Webb, Measurement of bubble dynamics on an enhanced boiling surface, Exp. Therm. Fluid Sci. 16 (1998) 177–186.

[7] G.E. Thorncroft, J.F. Klausner, R. Mei, An experimental investigation of bubble growth and detachment in vertical upflow and downflow boiling, Int. J. Heat Mass Transfer 41 (1998) 3857–3871.

[8] G.E. Thorncroft, J.F. Klausner, The influence of vapor bubble sliding on forced convection boiling heat transfer, ASME J. Heat Transfer 121 (1999) 73–79.

[9] C.P. Yin, Y.Y. Yan, T.F. Lin, B.C. Yang, Subcooled flow boiling heat transfer of R-134a and associated bubble characteristics in a horizontal annular channel, Int. J. Heat Mass Transfer 43 (2000) 1885–1896.

[10] M.M. Shah, Generalized prediction of heat transfer during subcooled boiling in annuli, Heat Transfer Eng. 4 (1983) 24–31.

[11] S.G. Kandlikar, Heat transfer characteristics in partial boiling, fully developed boiling, and significant void flow regions of subcooled flow boiling, ASME J. Heat Transfer 120 (1998) 395–401.

[12] K.E. Gungor, R.H.S. Winterton, A general correlation for flow boiling in tubes and annuli, Int. J. Heat Mass Transfer 29 (1986) 351–358.

[13] R.K. Shah, W.W. Focke, Plate heat exchangers and their design theory, in: R.K. Shah, E.C. Subbarao, R.A. Mashelkar (Eds.), Heat Transfer Equipment Design, Hemisphere, Washington, DC, 1988, pp. 227–254.

[14] A. Muley, R.M. Manglik, Experimental study of turbulent flow heat transfer and pressure drop in a plate heat exchanger with chevron plates, ASME J. Heat Transfer 121 (1999) 110–117.

[15] A. Muley, R.M. Manglik, H.M. Metwally, Enhanced heat transfer characteristics of viscous liquid flows in a chevron plate heat exchanger, ASME J. Heat Transfer 121 (1999) 1011–1017.

[16] B. Thonon, R. Vidil, C. Marvillet, Recent research and developments in plate heat exchangers, J. Enhanced Heat Transfer 2 (1995) 149–155.

[17] A.R. Khan, N.S. Baker, A.P. Wardle, The dynamic characteristics of a countercurrent plate heat exchanger, Int. J. Heat Mass Transfer 31 (1988) 1269–1278.

[18] G. Kreissig, H.M. Müller-Steinhagen, Frictional pressure drop for gas/liquid two-phase flow in plate heat changers, Heat Transfer Eng. 13 (1992) 42–52.

[19] C. Tribbe, H.M. Müller-Steinhagen, Gas/liquid flow in plate-and-frame heat exchangers – part I: pressure drop measurements, Heat Transfer Eng. 22 (2001) 5–11.

[20] C. Tribbe, H.M. Müller-Steinhagen, Gas/liquid flow in plate-and-frame heat exchangers – part II: two-phase multiplier and flow pattern analysis, Heat Transfer Eng. 22 (2001) 12–21.

[21] Y.Y. Yan, T.F. Lin, Evaporation heat transfer and pressure drop of refrigerant R-134a in a plate heat exchanger, ASME J. Heat Transfer 121 (1999) 118–127.

[22] Y.Y. Yan, H.C. Lio, T.F. Lin, Condensation heat transfer and pressure drop of refrigerant R-134a in a plate heat exchanger, Int. J. Heat Mass Transfer 42 (1999) 993–1006.

[23] S.J. Kline, F.A. McClintock, Describing uncertainties in single-sample experiments, Mech. Eng. 75 (1) (1953) 3–12.

[24] O. Zeitoun, M. Shoukri, Bubble behavior and mean diameter in subcooled flow boiling, ASME J. Heat Transfer 118 (1996) 110–116.